Impact of turbulence on high-precision ground-satellite frequency transfer with two-way coherent optical links

Clélia Robert* and Jean-Marc Conan
ONERA, The French Aerospace Lab, F-92322 Châtillon, France

Peter Wolf
SYRTE, Observatoire de Paris, PSL Research University, CNRS, Sorbonne Universités, UPMC Université Paris 06, LNE, 61 Avenue de l'Observatoire, F-75014 Paris, France

(Received 4 January 2016; revised manuscript received 18 February 2016; published 31 March 2016; corrected 7 July 2016)

Bidirectional ground-satellite laser links suffer from turbulence-induced scintillation and phase distortion. We study the impact of turbulence on coherent detection and the related phase noise that restricts time and frequency transfer precision. We evaluate the capacity to obtain a two-way cancellation of atmospheric effects despite the asymmetry between up- and downlink that limits the link reciprocity. For ground-satellite links, the asymmetry is induced by point-ahead angle and possibly the use, for the ground terminal, of different transceiver diameters, in reception and emission. The quantitative analysis is obtained thanks to refined end-to-end simulations under realistic turbulence and wind conditions as well as satellite kinematics. These temporally resolved simulations allow characterizing the coherent detection in terms of time series of heterodyne efficiency and phase noise for different system parameters. We show that tip-tilt correction on ground is mandatory at reception for the downlink and as a pre-compensation of the uplink. Besides, thanks to the large tilt angular correlation, the correction is shown to be efficient on uplink despite the point-ahead angle. Very good two-way compensation of turbulent effects is obtained even with the asymmetries. The two-way differential phase noise is reduced to 1rad^2, with the best fractional frequency stability below 2×10^{-17} after 1-s averaging time.

DOI: 10.1103/PhysRevA.93.033860

I. INTRODUCTION

Optical bi-directional links between ground stations and spacecraft in Earth or solar system orbits are of interest for a number of applications ranging from telecommunications to navigation, geodesy, time and frequency metrology, and fundamental physics [1–4]. Compared to radio frequency links, the optical links promise high data rates and low phase noise in long distance clock comparison or ranging measurements. In particular, low noise, long distance clock comparisons in Earth's orbit and in the solar system are of strong interest for experimental gravitation, relativistic geodesy, and time-frequency metrology [2–5]. The limiting effect for such optical links is likely to be atmospheric turbulence. We study its impact on two-way clock comparisons with a coherent detection, and quantify it by means of numerical simulations.

While many applications require clocks in space, the best present optical clocks can only be compared over continental distances at their full performance level, as demonstrated in optical fiber links [6,7]. Such long distance comparisons take advantage of two-way compensation schemes that allow mitigation of any source of phase noise that is reciprocal on the two channels. Free space optical links should allow a gain of more than 3 orders of magnitude in frequency transfer precision compared to radio-frequency links ($\Delta f/f = 10^{-18}$ instead of 10^{-15}). Despite turbulence that may limit this gain, promising performance on ground links has recently been obtained over kilometric horizontal distances [8–10]. Whether turbulence effects (reduction of signal, extinctions, phase noise, etc.) could be a limiting factor for high-precision ground-space two-way frequency transfer is the question we address in this paper.

We consider a coherent detection that is generally more sensitive to the signal and less sensitive to background light. Two criteria are essential for the performance of optical time-frequency comparisons: heterodyne efficiency (m) which characterizes the fractional loss of signal to noise ratio S/N and the phase noise (φ) on the phase modulation used to transfer the time or frequency information. Both criteria are impaired by turbulence. The first analysis of turbulence effects on coherent optical links, i.e., with heterodyne detection, has been performed by Fried [11]. He obtained an analytical expression of the mean of the heterodyne efficiency $\langle m\rangle$ in the presence of turbulence. Approximate distributions of m for a limited range of receiving apertures were then obtained through analytical developments [12]. Afterward, Monte Carlo simulations have been used to avoid questionable approximations on the aperture's spatial averaging and in turn give more accurate evaluation of heterodyne efficiency statistics [13,14]. These initial works assumed a phase only perturbation and were neglecting diffraction effects during the propagation; they, however, gave first-order evaluations of the gain brought by adaptive optics (AO). More recently Perlot [15] presented a very detailed analysis on coherent detection based on Monte Carlo simulations including scintillation effects with some approximations and using a simple AO correction on tip and tilt. His work was motivated by telecommunication applications. Other recent studies in free-space optical links [16,17] derived closed-form expressions for the probability density function of m with AO compensation. Note that these references only deal with the link S/N ratio via m. In the context of frequency transfer one has, however, to study phase noise

*clelia.robert@onera.fr

φ and its two-way compensation, the level of which depends of the reciprocal nature of φ.

Owing to the linear nature of wave propagation, one can show that the principle of reciprocity applies to propagation through turbulence [18–20]. Consequences of this principle on optical links, mainly in the context of free space optical telecommunications, have been studied by theoretical analysis [21–25] and through experimental demonstrations [8,9,26–28]. References [26–28] studied the link reciprocity experimentally in the context of incoherent detection for telecommunications. Closer to our work, Refs. [8,9] have recently studied two-way cancellation of turbulent effects on phase noise in frequency transfer links, along horizontal propagation paths with perfect overlap between the two channels.

In practice, there are several reasons that limit the link reciprocity in ground-satellite laser links: point ahead induced by the large satellite velocity, leading to a different line of sight for up- and downlink; another asymmetry is induced by the choice of different aperture sizes for reception and emission on ground, often motivated by technical considerations (available laser power on ground and on board, pointing requirements, stray light, etc.).

This article studies the impact of these asymmetries on phase noise compensation. We provide a quantitative evaluation of the residual phase noise $\Delta\varphi$ after two-way compensation, and in turn of the frequency stability $\Delta f/f$ in terms of Allan variance. Refined end-to-end simulations allow one to perform this quantitative analysis accounting for realistic turbulence and geometries. We use the reciprocity principle to model the bidirectional ground-satellite optical link using two downward plane waves propagating through the turbulence volume and separated by the point-ahead angle. We compute temporal series of m and φ for up- and downlinks, varying the turbulence conditions (turbulence strength, outer scale) and the aperture diameters of the ground transceiver, and we consider tip and tilt control to improve signal to noise ratio.

In summary, the major results of the present article concern three key topics: first, the assessment of tip-tilt correction efficiency especially for uplink in the presence of a large point ahead; second, the quantitative analysis of turbulence effects on two-way phase noise compensation in the presence of asymmetries between uplink and downlink (point-ahead angle and aperture differences); third, the evaluation of the effect of turbulence on frequency stability in two-way frequency transfer.

The asymmetries between uplink and downlink (point-ahead angle and aperture differences) give rise to only small values of $\Delta\varphi$ allowing for two-way frequency comparisons with exceptional stability in less than 1-s averaging time. The outline of the article is as follows. Section II exposes the necessary theoretical concepts, metrics of the coherent detection, and a review of reciprocity and adaptive optics aspects. Section III presents the turbulence propagation modeling and describes the numerical methods used in our simulations. Section IV presents the results: up- and downlink heterodyne efficiency and phase noise, two-way phase noise compensation, and the Allan variance. We discuss the influence of turbulent parameters in Sec. V and provide a comprehensive summary and conclusion in Sec. VI. Although the next sections are essential for an in-depth understanding of our work, the readers who are directly interested in our main results can go to Sec. IV.

II. THEORETICAL CONCEPTS AND METRICS FOR FREQUENCY TRANSFER

This section first defines the metrics used to qualify a coherent optical link impaired by atmospheric turbulence (see Sec. II A). Section II B then describes the relation between these metrics and the frequency transfer application. Section II C presents the theoretical concepts that govern link reciprocity and discusses the interest of adaptive optics in our context.

A. Effect of turbulence on heterodyne efficiency and phase noise

We first present the basic equations leading to the definition of the heterodyne efficiency in the presence of turbulence. The development of this section is based on the pioneering work of Fried [11]. We show the expressions for any kind of beam shapes, without restricting to the plane-wave case, and we introduce the notion of complex coupling.

In order to derive the heterodyne efficiency we first have to come back to the basics of the coherent detection. We start from two fields of form $E(\mathbf{r})\cos(\omega t+\phi(\mathbf{r}))$ (where $\mathbf{r}$ is the transverse two-dimensional spatial coordinate), denoted with subscript L for the local oscillator (LO), and denoted with subscript S for the signal. In a heterodyne detection, the diode current (in Ampere) at intermediate frequency $\frac{\omega_{\rm IF}}{2\pi}=\frac{\omega_S-\omega_L}{2\pi}$ is

$$i_{\rm IF}=\frac{e}{h\nu Z_0}\int \eta(\mathbf{r})E_L(\mathbf{r})E_s(\mathbf{r})\cos(\omega_{\rm IF}t+\Delta\phi(\mathbf{r}))d\mathbf{r}, \quad (1)$$

where $\Delta\phi(\mathbf{r})=\phi_S(\mathbf{r})-\phi_L(\mathbf{r})$ is the phase shift with respect to the local oscillator, $\eta(\mathbf{r})$ is the quantum efficiency of the detector (electrons/photon), Z_0 is the free space impedance (exactly 119.9169832π Ohm), and E_S and E_L are the signal and LO electric field amplitudes (in V/m) in the same polarization. In the following, we take the common assumption that the detector efficiency is independent of spatial coordinates, and the integral is performed on the aperture surface $\mathcal{A}$. In the presence of turbulence the signal field amplitude in Eq. (1) reads

$$E_s(\mathbf{r})=E_s\exp(\chi_S(\mathbf{r})), \quad (2)$$

where E_s is a constant, while $\chi_S(\mathbf{r})$ is the so-called log amplitude describing the field amplitude distribution, including beam shape and also scintillation effects induced by turbulence. Turbulent phase effects are of course included in the previously mentioned phase term $\phi_S(\mathbf{r})$. In the case of an LO amplitude in the form $E_L(\mathbf{r})=E_L\exp(\chi_L(\mathbf{r}))$, the current is

$$i_{\rm IF}=\frac{e\eta E_L E_s}{h\nu Z_0}\int_{\mathcal{A}}\exp[\chi_S(\mathbf{r})+\chi_L(\mathbf{r})]\times\cos[\omega_{\rm IF}t+\phi_S(\mathbf{r})-\phi_L(\mathbf{r})]d\mathbf{r}. \quad (3)$$

To get optimal performance of the heterodyne detection, we need a powerful LO to neglect the thermal noise. Under this assumption, the average LO current responsible for the

shot noise is

$$i_L = \frac{e\eta}{h\nu Z_0} E_L^2 \overline{\left(\int_{\mathcal{A}} \exp[\chi_L(\mathbf{r})] \cos[\omega_L t + \phi_L(\mathbf{r})] d\mathbf{r} \right)^2}, \quad (4)$$

where the over bar denotes from now on a time average over a duration much longer than the cosine period but much shorter than the turbulence evolution. The shot noise within a bandwidth Δf is equal to the square root of two times the average number of electrons in Δf. That is [2× Eq. (4)/$(e\Delta f)$]$^{1/2}$. The signal is equal to the average number of signal electrons in Δf. So the signal to noise power is [Eq. (3)/$(e\Delta f)$]^2/[2× Eq. (4)/$(e\Delta f)$] and we get the signal to noise ratio S/N,

$$S/N = \frac{\eta E_s^2 S}{2h\nu Z_0 \Delta f} \frac{\overline{\left(\int_{\mathcal{A}} \exp[\chi_S(\mathbf{r}) + \chi_L(\mathbf{r})] \cos[\omega_{\mathrm{IF}} t + \phi_S(\mathbf{r}) - \phi_L(\mathbf{r})] d\mathbf{r} \right)^2}}{\overline{\left(\int_{\mathcal{A}} \exp[\chi_L(\mathbf{r})] \cos[\omega_L t + \phi_L(\mathbf{r})] d\mathbf{r} \right)^2}}. \quad (5)$$

We define here the heterodyne efficiency m as the loss of signal to noise ratio compared to the unperturbed case, which corresponds to $\chi_{S0}(\mathbf{r})$ and ϕ_{S0}; hence the following expression for the heterodyne efficiency:

$$m = \frac{\overline{\left(\int_{\mathcal{A}} \exp[\chi_S(\mathbf{r}) + \chi_L(\mathbf{r})] \cos[\omega_{\mathrm{IF}} t + \phi_S(\mathbf{r}) - \phi_L(\mathbf{r})] d\mathbf{r} \right)^2}}{\overline{\left(\int_{\mathcal{A}} \exp[\chi_{S0}(\mathbf{r}) + \chi_L(\mathbf{r})] \cos[\omega_{\mathrm{IF}} t + \phi_{S0}(\mathbf{r}) - \phi_L(\mathbf{r})] d\mathbf{r} \right)^2}}. \quad (6)$$

Following [13], the formulation can be simplified by introducing the notion of complex fields:

$$m = \frac{|\int \mathcal{E}_L^*(\mathbf{r}) \mathcal{E}_S(\mathbf{r}) d\mathbf{r}|^2}{|\int \mathcal{E}_L^*(\mathbf{r}) \mathcal{E}_{S0}(\mathbf{r}) d\mathbf{r}|^2} = \frac{|\mathcal{C}|^2}{|\mathcal{C}^0|^2}, \quad (7)$$

where the complex fields, respectively, for the LO and the signal, are defined by $\mathcal{E}_L = E_L(\mathbf{r}) \exp[i\phi_L(\mathbf{r})]$, and $\mathcal{E}_S = E_S(\mathbf{r}) \exp[i\phi_S(\mathbf{r})]$. $\mathcal{E}_{S0}(\mathbf{r})$ is the signal complex field in the absence of turbulence. The integrals of the previous equation are called hereafter "complex couplings." They correspond to the overlap integrals between the incident signal and the local oscillator fields. The complex couplings, respectively, in the presence and in the absence of turbulence, are denoted $\mathcal{C}$ and $\mathcal{C}^0$. Equation (7) is again not specific to plane waves, and is valid for any type of wave. Note also that by definition $m = 1$ for the unperturbed case.

Reference [11] shows that the mean heterodyne efficiency $\langle m \rangle$ is asymptotically equal to $1/(D/r_0)^2$ for $D/r_0 \gg 1$, where r_0 is the Fried diameter characterizing the turbulence strength. Similarly to the case of astronomical imaging, $D \gg r_0$ leads to a strong impact of turbulence. High order AO correction may then be employed to correct the wavefront before the detection, so as to raise the mean heterodyne efficiency and reduce its fluctuations [14]. However, for $D \leqslant 2r_0$ or $3r_0$, a simple tip-tilt correction is generally sufficient [29]. This option is analyzed in this paper.

To quantify the effect of turbulence on long distance coherent optical links one has to quantify the mean heterodyne efficiency $\langle m \rangle$, but also its relative temporal fluctuations $\sigma_m^2/\langle m \rangle^2$ where σ_m^2 is the variance of m.

For clock comparison applications, a key additional parameter is the clock frequency stability. This implies to evaluate the temporal evolution of the phase noise, i.e., the phase of the beating signal at the intermediate frequency $\omega_{\mathrm{IF}}/(2\pi)$. This phase noise φ is by definition the phase of the complex coupling $\mathcal{C}$ that appears at the numerator of Eq. (7), hence:

$$\varphi = \arg(\mathcal{C}). \quad (8)$$

Note that in a strict sense there is no linear relation between the phase noise φ and the phase of the turbulent signal field ϕ_S. It is neither the signal phase at a given location, nor its pupil average (so-called piston $\langle \phi_S(\mathbf{r}) \rangle_{\mathrm{pupil}}$) or weighted average, the latter being only valid with a first-order development of $\exp(i\phi_S)$ [30,31]. A second-order development of the complex exponential, however, exhibits cross-terms between the turbulent phase modes: piston, tip-tilt, and higher orders. By removing tip and tilt, the phase noise should be closer to a piston since cross-terms then cancel out. We come back to the physical nature of the phase noise in Sec. IV D.

From Eqs. (7) and (8) we see that heterodyne efficiency and phase noise are derived from the same key quantity: the complex coupling $\mathcal{C}$ between the turbulent signal and local oscillator fields. The properties of this complex coupling are discussed in the following paragraphs and the context of frequency transfer is also recalled.

B. Frequency transfer in two-way coherent optical links

In the present work we consider the comparison of two clocks through a two-way heterodyne optical link between two terminals T_1 and T_2. Their reception and emission pupils are, respectively, located in a plane Π_1 (coordinates $\mathbf{r_1}$) and a plane Π_2 (coordinates $\mathbf{r_2}$), assumed to be perpendicular to the line of sight. Figure 1 gives a principle sketch of the ground-space optical link configuration with its point ahead. The turbulence volume is concentrated near the ground terminal, say T_1, and perturbs the optical propagation. As shown in Sec. II A, the key quantity that characterizes the link is the complex coupling. Respectively, for each terminal, the complex coupling at a given time reads

$$\mathcal{C}_1 = \int \mathcal{E}_{1L}^*(\mathbf{r_1}) \mathcal{E}_{1S}(\mathbf{r_1}) d\mathbf{r_1}, \quad (9)$$

$$\mathcal{C}_2 = \int \mathcal{E}_{2L}^*(\mathbf{r_2}) \mathcal{E}_{2S}(\mathbf{r_2}) d\mathbf{r_2}, \quad (10)$$

where $\mathcal{E}_{1L}$ and $\mathcal{E}_{2L}$ are the complex fields of the local oscillator of T_1 and T_2, while $\mathcal{E}_{1S}$ and $\mathcal{E}_{2S}$ are the signal complex fields received, respectively, in T_1 and T_2 pupils.

The comparison of two clocks on each side of the link is affected by phase noise induced by turbulence. With two-way

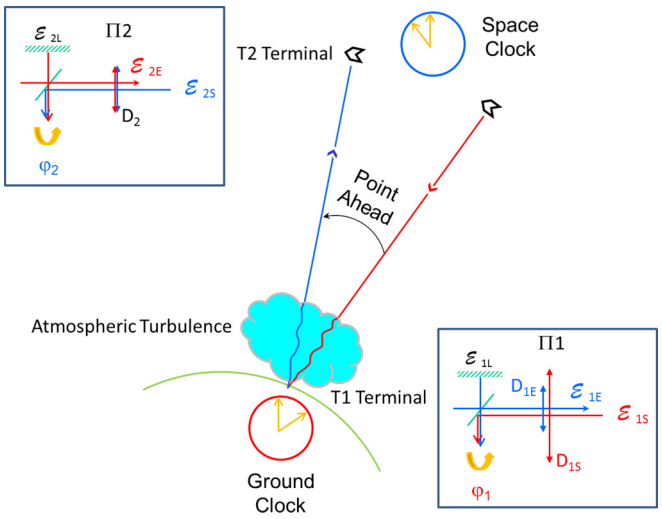

FIG. 1. Principle of clock comparison using coherent optical links. The phase noises φ_1 and φ_2 are measured at intermediate frequency ω_{IF} on both terminals T_i, where $i = 1,2$ for ground and space, respectively. Received or transmitted electromagnetic fields are denoted $\mathcal{E}_{iS}$ and $\mathcal{E}_{iE}$. They pass through the aperture diameters denoted D_i located in the planes Π_i. Local oscillator fields are denoted $\mathcal{E}_{iL}$.

compensation techniques one is, however, only sensitive to differential effects, namely to the half difference of phase noise: $\Delta\varphi = (\varphi_1 - \varphi_2)/2 = [\arg(\mathcal{C}_1) - \arg(\mathcal{C}_2)]/2$, meaning that any phase noise on the links that is reciprocal cancels in the two-way clock comparison [32].

Clearly, the frequency transfer precision will be ultimately driven by the level of link reciprocity that characterizes the similarity of the complex couplings of each terminal. Section II C now describes the physical principles that govern reciprocity properties of the complex coupling and related phase noise.

C. Principle of reciprocity for two-way ground-satellite optical links modeling

Before discussing the link reciprocity, let us come back to the general principle of reciprocity in propagation through turbulence, a well-known physics property ([18–20]). In short, wave propagation being a linear process, there is a unique functional that allows one to describe by an integral equation the forward propagation of the complex field from a plane Π_1 to a plane Π_2, and the backward propagation from Π_2 to Π_1:

$$\mathcal{E}_{2S} = \int h(\mathbf{r_1},\mathbf{r_2})\mathcal{E}_{1E}(\mathbf{r_1})d\mathbf{r_1}, \tag{11}$$

$$\mathcal{E}_{1S} = \int h(\mathbf{r_1},\mathbf{r_2})\mathcal{E}_{2E}(\mathbf{r_2})d\mathbf{r_2}, \tag{12}$$

where, for the forward propagation, $\mathcal{E}_{1E}$ is the emitted complex field in plane Π_1 and $\mathcal{E}_{2S}$ the received complex field in plane Π_2, $\mathcal{E}_{2E}$ and $\mathcal{E}_{1S}$ being the emitted and received fields for the backward propagation. $h(\mathbf{r_1},\mathbf{r_2})$ is the functional that characterizes the propagation medium, here the propagation through a given turbulence state at a given time. This property is sometimes referred to as the "extended Huygens-Fresnel principle" [23]. Note that it does not require assumptions on the turbulence strength, and therefore applies even in strong perturbation regimes. The only implicit assumption is that turbulence does not evolve during the time of propagation through the turbulent volume.

1. *Implications on link reciprocity*

Consequences of this principle on optical links have been the object of theoretical studies [21–25] mainly in the context of free space optical telecommunications. For a comprehensive understanding of the implications on frequency transfer, the main theoretical results are presented from the perspective of coherent links and their related phase noise.

From Eqs. (12) and (9), one can easily show that

$$\mathcal{C}_1 = \int \mathcal{E}^*_{1L}(\mathbf{r_1})\left(\int \mathcal{E}_{2E}(\mathbf{r_2})h(\mathbf{r_1},\mathbf{r_2})d\mathbf{r_2}\right)d\mathbf{r_1}. \tag{13}$$

While Eqs. (11) and (10) lead to

$$\mathcal{C}_2 = \int \mathcal{E}_{1E}(\mathbf{r_1})\left(\int \mathcal{E}^*_{2L}(\mathbf{r_2})h(\mathbf{r_1},\mathbf{r_2})d\mathbf{r_2}\right)d\mathbf{r_1}, \tag{14}$$

where integral orders have been exchanged to obtain a reciprocal expression of $\mathcal{C}_2$, expressed in the plane Π_1. The complex couplings at both sides of the optical link can therefore be expressed as overlap integrals in the T1 aperture plane. They both involve complex fields resulting in the propagation from T2 to T1. These propagated fields, the terms between parentheses, correspond on one hand to the natural propagation of $\mathcal{E}_{2E}$, the field emitted by T2, and on the other hand to a fictive back propagation through turbulence of $\mathcal{E}^*_{2L}$, the T2 local oscillator complex conjugate.

It is interesting to note that in the particular case where $\mathcal{E}_{1E} = \mathcal{E}^*_{1L}$ and $\mathcal{E}_{2E} = \mathcal{E}^*_{2L}$, symmetry on each terminal between the emission and the local oscillator, then $\mathcal{C}_1$ is equal to $\mathcal{C}_2$. Under these conditions the link reciprocity is perfect, meaning that both sides of the link have strictly identical heterodyne efficiency and phase noise.

Again, these developments are simply a transposition to heterodyne detection of the work of Shapiro (see [24] and references therein), where we have local oscillator modes in place of fiber modes, and where our expressions deal with complex coupling instead of its square modulus, since we care about phase noise in our application.

References [23–25] draw various implications of these reciprocity properties depending on the link geometry. Note that the previous equations are not specific to the ground-satellite configuration, and we now restrict our discussion to this particular case. Such a link has several specificities:

(1) Very long distance of propagation (thousands to tens of thousands of kilometers), hence clearly corresponding to a far field case.

(2) Turbulent volume is concentrated in the first few tens of kilometers near ground; note that the time of propagation through turbulence remains very short (around 100 μs), even if the total propagation time to the satellite is large.

(3) High satellite velocity leads to a point-ahead angle between the downward and upward beams.

Items 1 and 2 imply that the turbulence coherence area in the satellite plane is much larger than T2 pupil size. Therefore,

in the previous expressions, on can neglect the dependence in $\mathbf{r_2}$ of $h(\mathbf{r_1},\mathbf{r_2})$, and approximate it by $h(\mathbf{r_1},\mathbf{0})$ [23]. The complex couplings then now read

$$\mathcal{C}_1 = \int \mathcal{E}^*_{1L}(\mathbf{r_1}) h(\mathbf{r_1},\mathbf{0}) d\mathbf{r_1} \left(\int \mathcal{E}_{2E}(\mathbf{r_2}) d\mathbf{r_2} \right), \quad (15)$$

$$\mathcal{C}_2 = \int \mathcal{E}_{1E}(\mathbf{r_1}) h(\mathbf{r_1},\mathbf{0}) d\mathbf{r_1} \left(\int \mathcal{E}^*_{2L}(\mathbf{r_2}) d\mathbf{r_2} \right). \quad (16)$$

In both expressions the terms between parentheses are constant factors independent of turbulence. This implies that the analysis of turbulent effects does not depend on T2 modes. Looking at Eq. (12), one can see that $h(\mathbf{r_1},\mathbf{0})$ would be the received field on ground if the emission field $\mathcal{E}_{2E}(\mathbf{r_2})$ were a Dirac $\delta(\mathbf{r_2})$; it therefore corresponds to the downward propagation of a plane wave through turbulence. The fact that one can model the downlink with a downward plane-wave propagation, neglecting the Gaussian nature of the beam coming from the satellite, is actually a usual approximation in ground-space optical links, both for incoherent and coherent detection (see, for instance, Chapter 9 in Ref. [33]). The reciprocal expression of $\mathcal{C}_2$ shows that, based on the same approximation, the uplink coupling can also be calculated from this downward plane wave. Actually, this is true only when neglecting the point-ahead effect [23] mentioned in item 3. Accounting for point ahead is, however, easy and only implies that $h(\mathbf{r_1},\mathbf{0})$ is not exactly the same term in Eqs. (15) and (16): It corresponds to the result of the propagation, through the same turbulent volume, of two downward plane waves with two propagation directions separated by the point-ahead angle. Say on-axis for the downlink in Eq. (15) and off-axis at point ahead for the uplink in Eq. (16). There is therefore no need to simulate the upward propagation of a Gaussian beam.

To summarize, two asymmetries affect the link reciprocity of such a link: the potential difference between reception and emission modes on the ground terminal, and the point-ahead effect. The evaluation of link reciprocity in realistic ground-satellite conditions is the object of Sec. IV.

2. *Correction and pre-compensation by adaptive optics*

The developments presented in Sec. II C 1 remain valid in the presence of AO, that can be used for either correction at reception, or for pre-compensation at emission [24]. AO simply adds phase terms to emission or local oscillator fields in the previous expressions. Besides, in the case of ground-satellite links, Eqs. (15) and (16) clearly tell that a phase correction can be beneficial on the ground terminal to partly compensate the turbulent phase effects in $h(\mathbf{r_1},\mathbf{0})$. However, in these equations, the satellite modes (emission and local oscillator) only give a constant factor decoupled from turbulence effects. AO is therefore of no interest on-board. This well-known property [23,24] is again a consequence of the fact that the turbulence coherence area in the satellite plane is much larger than T2 aperture size.

In the present paper we only consider tip-tilt both to correct the incoming downlink beam, and to pre-compensate the uplink. From Eqs. (15) and (16), one can infer that the optimum tip-tilt correction should be deduced from the on-axis plane wave for the downlink, and from the off-axis plane wave at point ahead for the uplink. Unfortunately there is no off-axis beacon available in the point-ahead direction; tip-tilt correction can therefore only be estimated on the downlink beam (on-axis plane wave). The same tip-tilt correction is then applied to the downlink and uplink. One understands that tilt anisoplanatism may limit the correction efficiency for the uplink. And more generally, point ahead limits the capacity to efficiently pre-compensate the uplink beam by AO [22].

As we have seen, the reciprocity principle is a powerful tool to analyze the link properties, and it also simplifies numerical modeling since up- and downlink performance can be deduced from the sole propagation of two downward plane waves. Although out of the scope of the present paper, this would be of particular interest to carry out parametric studies of the uplink AO pre-compensation through simulations. Propagation of the off-axis plane wave through turbulence can indeed be performed independently of the AO correction. The AO strategy can then be studied afterward by applying corrections on the pre-computed propagated fields. A true uplink propagation of a Gaussian beam with pre-compensation would require a specific propagation for each choice of the AO correction phase.

We now have to quantify the heterodyne efficiency, and the gain brought by tip-tilt correction. We have also to evaluate the impact of the bi-directional link asymmetries on the link reciprocity. For this purpose, we use refined Monte Carlo end-to-end simulations that are described in the next section.

III. MODEL AND METHODS

A. Turbulence propagation modeling

PILOT is our numerical wave-optics tool based on Monte Carlo split-step propagation: simulation of optical propagation through discrete turbulent random phase screens based on Fresnel propagation. This code is routinely used for endo-atmospheric applications or astronomy [34], and ground-space telecommunications modeling [35,36]. Since wave optics does not rely on hypotheses on the turbulence regime, this also allows us to cover all satellite elevations including those with strong perturbations.

Figure 2 displays a sketch describing the optical propagation through turbulence for ground-space optical links. The turbulence volume can be described by discrete layers (perpendicular to the line of sight) introducing a phase perturbation on the optical beam. Temporal evolution is obtained by translating

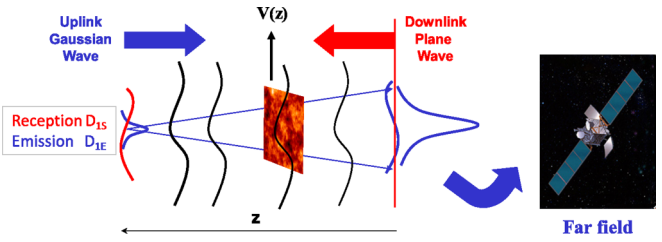

FIG. 2. Turbulence and propagation modeling on ground-space optical link. The wavy black lines represent the moving phase screens with an apparent wind speed $V(z)$ where z is the propagation axis. The red lines show the downlink plane wave. The blue Gaussian ones show the uplink wave. Line of sight is artificially set horizontal on the sketch. Photograph of the satellite from Ref. [37].

the phase screens, the so-called Taylor hypothesis, with an apparent wind speed accounting for the transverse component of the natural wind added to the apparent wind induced by the satellite tracking. We assume Von Kármán statistics for the turbulent phase in a given layer. Turbulence strength is characterized locally by the so-called "refractive index structure parameter" denoted C_n^2 and the turbulence outer scale L_0. Even though this model is sometimes questioned especially for near ground observations (see, for instance, [10]), it is still a standard model for earth-space propagation. Besides, the Taylor hypothesis is fully relevant for distant layers where the wind induced by satellite tracking is dominant.

The integrated strength along the line of sight of these wavefront distortions is quantified by the Fried parameter r_0, always expressed in plane wave in this article. Even if turbulence induces locally phase only perturbations, diffraction effects during the beam propagation progressively transform phase effects in amplitude perturbations, the so-called scintillation, with a wavelength. Phase and scintillation effects of course limit the heterodyne efficiency and induce phase noise.

As shown in Sec. II C 1, up- and downlink performance can be deduced from the propagation, through the same turbulent volume, of two downward plane waves along two axes separated by the point-ahead angle. This is performed by running the wave-optics propagation code PILOT at the working wavelength of $\lambda = 1064$ nm. The turbulent vertical distribution corresponds to a C_n^2 profile of an astronomical site with moderate turbulence. It covers the [0,20 km] altitude range described by a Hufnagel-Valley profile above the boundary layer (at about 1.5 km) linked to the Monin-Obukhov similitude laws below. We use 10 phase screens spread nonuniformly in altitude. Five of them are put in the first km, inside the boundary layer, to sample the significant turbulence. The other five are placed at 4, 6, 10, 14, and 18 km. The r_0 (plane wave) is indicated for an oblique line of sight with 20° elevation. We study a moderate turbulence condition with $r_0 = 13$ cm. The isoplanatic angle is $\approx 25\ \mu$rad in these conditions. We set an outer scale $L_0 = 8$ m which is a realistic value [38]. Furthermore, after having varied L_0 on a 1- to 25-m range [39], we found that the two first moments of the heterodyne efficiency m do not evolve beyond $L_0 = 8$ m. Section V discusses the influence of turbulence parameters: the outer-scale value and a stronger turbulence with $r_0 = 5$ cm.

B. Practical implementation

Our propagation code provides time series of the electromagnetic fields for the two plane-wave downward propagations, respectively, on-axis and off-axis at point ahead. Equations (15) and (16) are then used to compute the complex coupling time series $\mathcal{C}_1(t)$ and $\mathcal{C}_2(t)$. We then derive link metrics such as the heterodyne efficiency and the phase noise of the signal at the intermediate frequency [see Eqs. (7) and (8)], respectively, the squared modulus of the complex coupling and its argument:

$$m_i(t) = \frac{|\mathcal{C}_i(t)|^2}{\left|\mathcal{C}_i^0(t)\right|^2}, \tag{17}$$

$$\varphi_i(t) = \arg(\mathcal{C}_i(t)), \tag{18}$$

where i is the terminal number (1 or 2), and $\mathcal{C}_i^0$ is the complex coupling of terminal i in the absence of turbulence. In practice to avoid phase jumps of 2π, we will proceed by successive increments:

$$\varphi_i(t+dt) - \varphi_i(t) = \arg(\mathcal{C}_i(t+dt)\mathcal{C}_i^*(t)). \tag{19}$$

The cumulative sum on all instants of the phase increment in Eq. (19) provides the phase noise temporal trajectory.

Simulations can include full tip-tilt correction at the ground receiver aperture for the downlink. Following Sec. II C 2, the same tip-tilt is used as a pre-compensation of the uplink at the ground emitter. The correction of tip and tilt is implemented in simulations as explained hereafter. The phase is extracted from the instantaneous turbulent electromagnetic field at the pupil. Then it is projected on Zernike polynomials (defined on the relevant aperture diameter) to get the modal coefficients of the tip and tilt. As the phase extraction provides a version of the phase modulo 2π, a step of unwrapping is added to the process before the projection. This tip-tilt is subtracted to the turbulent phase as a correction that is therefore ideal: no sensing noise, and correction without delay. It still represents a case with good signal-to-noise ratio and with a correction loop of high temporal bandwidth. These assumptions are sufficient for our present purposes, a more realistic AO system being relegated to future work.

At the end, temporal series of heterodyne efficiency and phase noise allow us to quantify, for different scenarios, the link performance including extinctions, link reciprocity together with two-way phase noise compensation, and Allan variances. The results are presented in the next section.

IV. PERFORMANCE EVALUATION FOR FREQUENCY TRANSFER

This section is dedicated to the performance evaluation of a two-way optical link for high-precision frequency transfer in moderate turbulence conditions. Section IV A first describes the simulation conditions. Section IV B gives an overview of the heterodyne efficiency statistics for down- and uplink, including its dependence with aperture size, tip-tilt correction, and point ahead. Section IV C details the downlink characteristics in terms of temporal trajectory of the heterodyne efficiency and of the phase noise. Section IV D analyzes the uplink temporal series, and the nature of the phase noise. Section IV E evaluates how link asymmetries affect the efficiency of two-way phase compensation and quantifies the expected frequency stability in terms of modified Allan variance.

A. Simulation conditions and system parameters

The satellite position is taken at perigee: Distance to the satellite is $z = 3200$ km, and velocity on its orbit is $v = 9$ km/s (component transverse to the line of sight). Perigee corresponds to a worst case in terms of point ahead: The point-ahead angle is here paa $= 60\ \mu$rad. We recall that the elevation of the line of sight is 20°.

As mentioned in Secs. II C 1 and III A, the up- and downlink performance can be deduced from time series of complex electromagnetic fields resulting in the downward propagation of two plane waves separated by the point-ahead angle. Our

propagation code PILOT is used to simulate two such time series corresponding to 8000 turbulent field occurrences. The duration of the series is 8 s with 1-ms sampling steps. In the next subsections we consider the moderate turbulence condition described in Sec. III A ($r_0 = 13$ cm).

The study is performed for two diameter values (0.15 or 0.40 m), corresponding either to the downlink ground receiver aperture (D_{1S}), or to the uplink ground emission aperture (D_{1E}). Both the ground LO and the uplink emission beam are considered Gaussian with the usual truncation rule: Waist w_0 is one-third of the considered aperture. Having large apertures may be of interest for link budget considerations, especially for ground reception since laser power on board is generally limited. As mentioned in Sec. II A one, however, expects a stronger impact of turbulence with larger apertures. We finally recall that, for what concerns turbulence and as shown in Sec. II C 1, link performance is independent of the choice of the satellite terminal geometry (apertures, beam size).

B. Heterodyne efficiency versus system parameters

We study here the influence of the ground transceiver diameters and of point ahead on heterodyne efficiency statistics: mean value $\langle m \rangle$ and relative fluctuations $\sigma_m^2/\langle m \rangle^2$. We consider both full turbulence and tip-tilt control cases. In the absence of point ahead, we recall that up- and downlink have by construction identical performance, hence the same heterodyne efficiency, when considering the same modes (diameter and waist) for emission and LO on the ground terminal (see Sec. II C 1).

Heterodyne efficiency statistics are summed up in Table I. For an aperture diameter of 0.40 m and without tip-tilt control, turbulence has a strong impact on heterodyne efficiency: low mean and large relative fluctuations, both for up- and downlinks. Tip-tilt control brings a significant gain: increase of the mean value and strong reduction of the fluctuations. Turbulence has a smaller impact with an aperture diameter reduced to 0.15 m, since D/r_0 is smaller, but tip-tilt control remains very valuable in this case.

Applying downlink tip-tilt to the pre-compensate uplink is efficient despite point ahead. Mean value is, for instance, only reduced by a few percent: In Table I please compare first, the cases with the superscript (b) and (d), and second the cases (c) and (e). The slight reduction of performance is caused by tip-tilt anisoplanatism that induces a difference between on-axis and off-axis tip-tilt at point ahead. The fact that this effect is minor may seem surprising since the point-ahead angle is larger than the isoplanatic angle in our case. One has, however, to remember that the isoplanatic angle is not a relevant parameter to describe the modal normalized angular correlations of Zernike modes [40]. Tip-tilt is known to have a large angular correlation (see, for instance, Fig. 3 in [34]): In our case the normalized correlation is better than 95% at the point-ahead angle.

TABLE I. Mean heterodyne efficiency $\langle m \rangle$ and its relative fluctuation $[\sigma_m^2/\langle m \rangle^2]$ for the up- and downlinks, with and without tip-tilt correction, for two ground aperture diameters D. Performance of the uplink is given with and without point ahead.

		Downlink and uplink w/o point ahead	Uplink and point ahead
$D = 0.40$ m	Turbulent	[a] 0.18 [0.84]	0.18 [0.84]
	Tip-tilt control	[b] 0.53 [0.07]	[d] 0.51 [0.08]
$D = 0.15$ m	Turbulent	0.60 [0.14]	0.60[0.14]
	Tip-tilt control	[c] 0.84 [0.01]	[e] 0.78 [0.03]

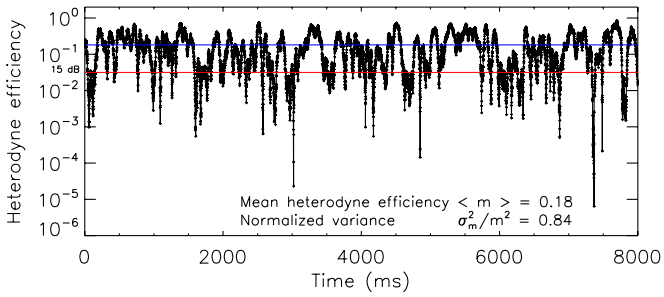

FIG. 3. Turbulent downlink time series of heterodyne efficiency along an 8-s duration sampled every 1 ms. The red (lower) straight line shows the detection threshold. The blue (upper) straight line shows the mean heterodyne efficiency $\langle m \rangle$. $D_{1S} = 0.40$ m. This case is labeled (a) in Table I.

Mean heterodyne efficiency $\langle m \rangle$ and its relative fluctuations $\sigma_m^2/\langle m \rangle^2$ are key parameters to characterize the link budget. However, they do not inform on the potential presence of extinctions. The next paragraphs discuss this point through the display of a temporal series of heterodyne efficiency. They also present associated phase noise trajectories.

C. Downlink with and without tip-tilt correction

We provide here a time series of the downlink heterodyne efficiency and phase noise, successively under full turbulence and with tip-tilt control; in the latter case we consider both receiver diameters $D_{1S} = [0.15, 0.40]$ m (cases (a), (b), and (c) of Table I).

To maintain reasonable signal-to-noise ratio, we set a "conservative" extinction threshold corresponding to a 15-dB loss induced by turbulence on the heterodyne efficiency. This level is indicated in red in Figs. 3–5. In the absence of correction (Fig. 3), and for the 0.40-m aperture, this criterion is far from being met: One is faced with very frequent and very

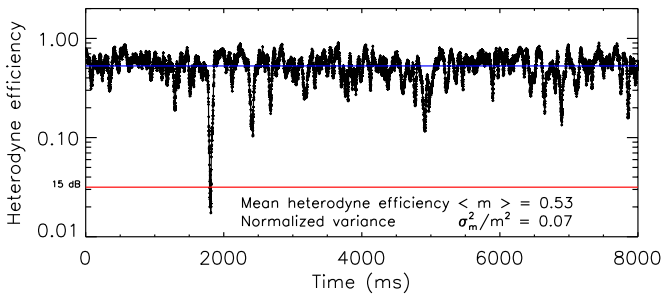

FIG. 4. Tip-tilt controlled downlink time series of heterodyne efficiency along an 8-s duration sampled every 1 ms. The red (lower) straight line shows the detection threshold. The blue (upper) straight line shows the mean heterodyne efficiency $\langle m \rangle$. $D_{1S} = 0.40$ m. This case is labeled (b) in Table I.

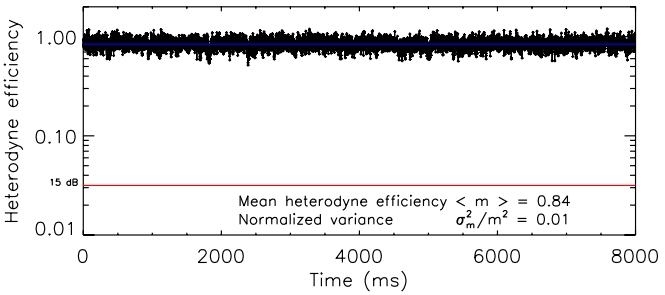

FIG. 5. Same description as in Fig. 4 for $D_{1S} = 0.15$ m. This case is labeled (c) in Table I.

deep extinctions (S/N loss exceeding 50 dB in some cases), preventing one from keeping track of the signal on durations longer than a few 100 ms. Tip-tilt correction brings a huge gain in that respect: Fig. 4 shows a single extinction, slightly below the threshold, on the 8-s duration. Heterodyne efficiency is of course again improved when considering a smaller aperture (0.15 m, still with tip-tilt control, in Fig. 5). Although not shown here, we examined the full turbulence case with 0.15 m aperture: Heterodyne efficiency exhibits less severe, just at the limit of the 15-dB threshold, but still frequent extinctions. Tip-tilt control is therefore mandatory to maintain reasonable signal-to-noise ratio, even at astronomical sites with moderate turbulence.

Concerning phase noise, its trajectory is significantly modified as we set the tip-tilt control, even if the variance remains on the same order (see Fig. 6 displayed for the aperture $D_{1S} = 0.40$ m). As mentioned in Sec. II A, all phase modes contribute to phase noise; it is therefore not surprising that tip-tilt control modifies the phase noise trajectory. Minor differences are observed on the tip-tilt controlled trajectories when going from 0.40- to 0.15-m aperture (see Fig. 7). We come back to these results and to the nature of the phase noise at the end of Sec. IV D.

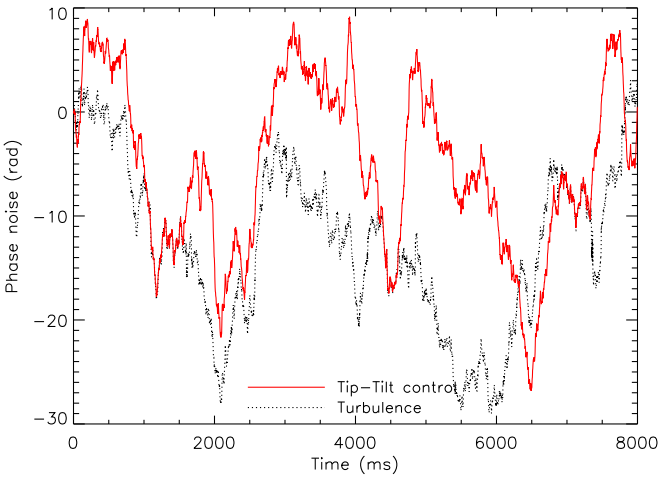

FIG. 6. Downlink time series of phase noise along an 8-s duration sampled every 1 ms. Receiver aperture $D_{1S} = 0.40$ m. Comparison between a turbulent case (dashed black curve, variance 61.9 rad^2) and a tip-tilt control one (solid red curve, variance 65.2 rad^2). These cases are, respectively, labeled (a) and (b) in Table I.

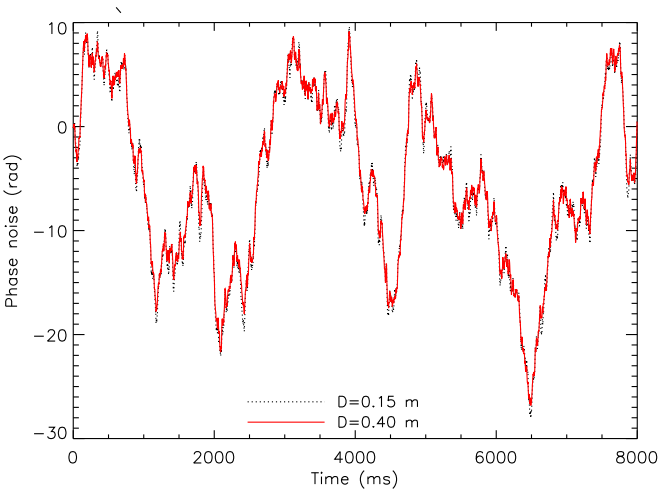

FIG. 7. Tip-tilt controlled downlink time series of phase noise along an 8-s duration sampled every 1 ms. Comparison between a small aperture case (dashed black curve, variance 66.7 rad^2) and a large aperture one (solid red curve, variance 65.2 rad^2). These cases are labeled (b) and (c) in Table I, respectively.

D. Uplink with tip-tilt pre-compensation

We analyze now the heterodyne efficiency and phase noise time series of the uplink. In all cases we apply downlink tip-tilt to pre-compensate the uplink, since it has been shown in the previous section to be efficient despite pointing ahead and mandatory to avoid extinctions. We consider the two emitter diameters $D_{1E} = [0.15, 0.40]$ m, and also take into account point ahead [cases (d) and (e) of Table I]. Comparison with no point ahead is presented in the analysis of differential phase noise in Sec. IV E.

Figure 8 shows the heterodyne efficiency evolution for the largest emitter's diameter $D_{1E} = 0.40$ m. It is very similar in shape to downlink's one (compare with Fig. 4), still with a single, shallow extinction in the 8-s duration. With a careful look, one can still see a slight and rather systematic reduction of m compared to downlink, leading to the loss of 2 percentage points on the mean value [cases (b) and (d) of Table I]. As explained in Sec. IV B, this performance reduction is due to tilt anisoplanatism.

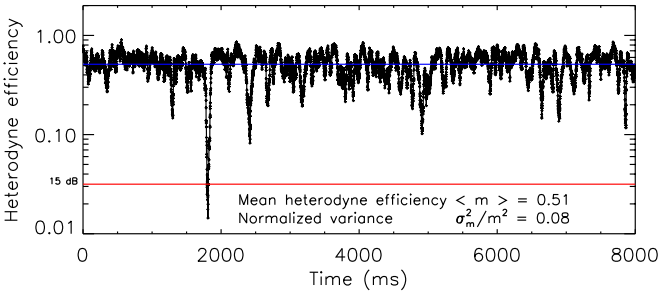

FIG. 8. Tip-tilt controlled uplink time series of heterodyne efficiency along an 8-s duration sampled every 1 ms. The red (lower) straight line shows the detection threshold. The blue (upper) straight line shows the mean heterodyne efficiency $\langle m \rangle$. $D_{1E} = 0.40$ m. This case is labeled (d) in Table I.

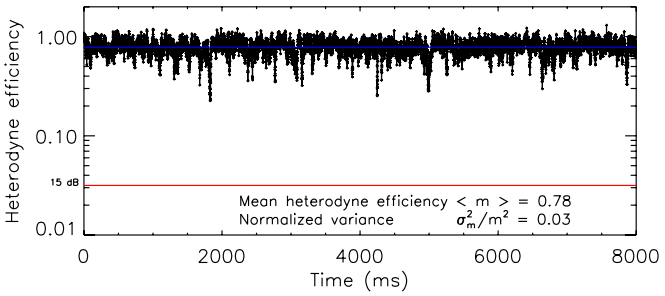

FIG. 9. Same description as in Fig. 8 for $D_{1E} = 0.15$ m. This case is labeled (e) in Table I.

The results with emission diameter $D_{1E} = 0.15$ m, are shown in Fig. 9, leading to similar conclusions: The time series are close to those of the downlink with the same aperture, the loss in heterodyne efficiency being only slightly more important here (corresponding to a loss of 6 percentage points in the mean between cases (c) and (e) of Table I). In any case, as already mentioned in the previous section, reducing the diameter improves performance; heterodyne efficiency is better on average and also more steady.

Concerning phase noise, one can note that the time series obtained with $D_{1E} = 0.15$ m and $D_{1E} = 0.40$ m (Fig. 10) are very similar. The phase noise time series corresponding to $D_{1E} = 0.40$ m is also very similar to that of the downlink (compare with the red curve in Fig. 7). This high degree of similarity gives evidence of a good link reciprocity despite point ahead. This aspect is analyzed in detail in Sec. IV E.

We have also computed for comparison the piston time series on the off-axis plane wave at point ahead for the two apertures (see Fig. 11). One can see first that piston trajectory is not very sensitive to the aperture value, and second that piston and phase noise are very much alike. The first point is related to the fact that piston variance is mainly driven by the key parameter L_0/r_0. The second aspect is also not surprising

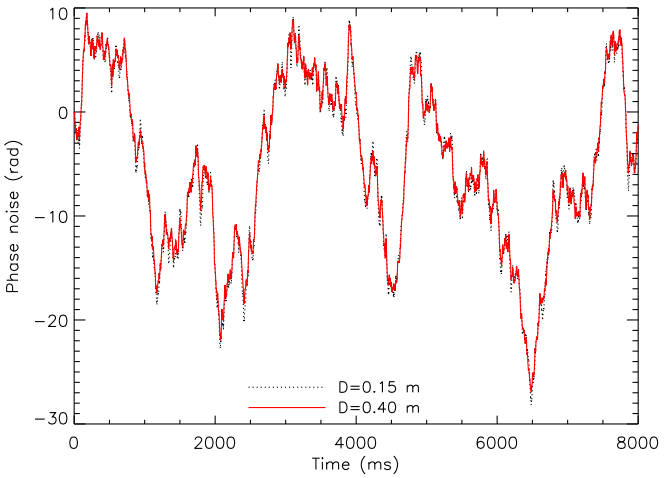

FIG. 10. Tip-tilt controlled uplink time series of phase noise along an 8-s duration sampled every 1 ms. Comparison between a small aperture case (dashed black curve, variance 66.7 rad^2) and a large aperture one (solid red curve, variance 65.2 rad^2). These cases are labeled (d) and (e) in Table I, respectively.

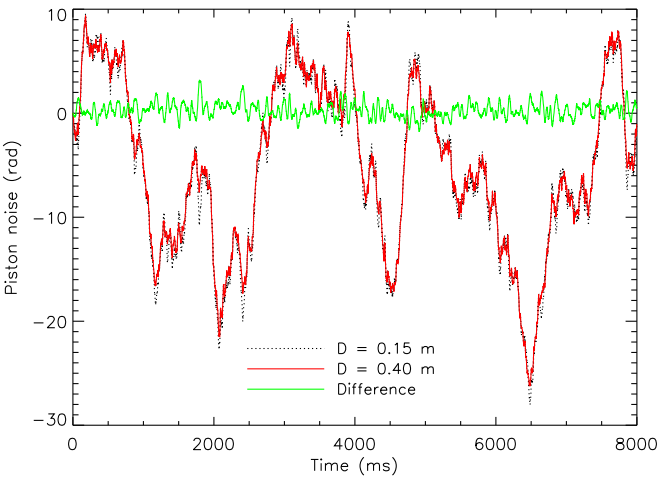

FIG. 11. Piston time series of phase noise along an 8-s duration sampled every 1 ms. Comparison between two aperture diameters $D = 0.15$ m (dashed black line) and $D = 0.40$ m (solid red line). Variances are, respectively, 66.5 rad^2 and 63.9 rad^2. The variance of the difference [green (light gray) line] is 0.51 rad^2.

since the tip-tilt control cancels out all cross-terms related to tip-tilt, phase noise being therefore closer to the piston.

For more insight, we have computed the temporal power spectral density (PSD) of piston and phase noise (not shown here). The piston PSD has the standard structure: $-8/3$ power law at low temporal frequencies, a cutoff, and a sharp decrease with a $-17/3$ power law [41]. The tip-tilt controlled phase noise PSD also follows a $-8/3$ power law at low temporal frequencies, confirming its similarity with piston, but it has a slightly larger high frequency content. This confirms that the phase noise is not a pure piston: Higher phase orders are also involved, and scintillation effects may also contribute. Note that this comparison to piston is developed in uplink phase noise, but it actually also applies to the downlink case.

E. Two-way phase noise compensation

High performance clock comparison techniques use two-way phase noise compensation to cancel out effects that are reciprocal in the two channels. Reciprocity of turbulent phase noise is, however, not perfect in the presence of link asymmetries. There are two sources of asymmetry in our case: the point ahead effect, and the possible difference of the ground terminal reception and emission apertures (see Sec. II C 1). We therefore evaluate, in this paragraph, the differential phase noise, between the down- and uplink, that ultimately limits frequency transfer precision. We also quantify the expected frequency stability in terms of the modified Allan variance. All the results are obtained with tip-tilt control.

The following graphs (Figs. 12–14) display the phase noise of the down- and uplink as well as their difference. We first consider individually the two sources of asymmetry: point ahead with symmetric apertures ($D_{1E} = D_{1S} = 0.40$ m) in Fig. 12; asymmetric apertures ($D_{1E} = 0.15$ m, $D_{1S} = 0.40$ m); and point-ahead angle artificially set to zero in Fig. 13. We see that the up- and downlinks are highly correlated (i.e., good reciprocity) leading in both cases to differential phase noise

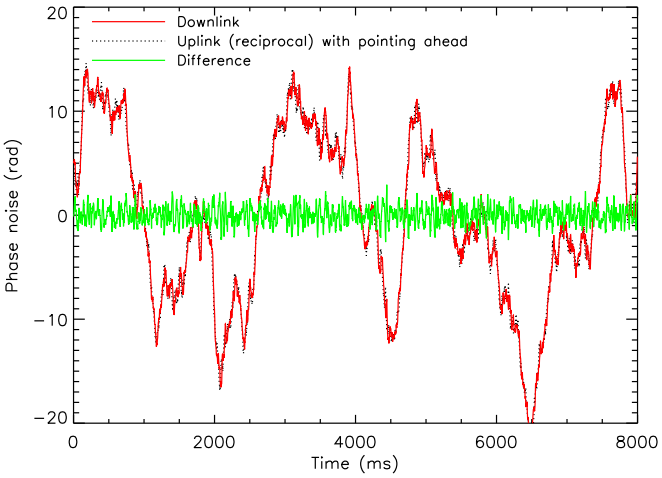

FIG. 12. Two-way compensation on phase noise in the case of symmetric apertures ($D_{1E} = D_{1S} = 0.40$ m) with point ahead and with tip-tilt correction. Comparison between downlink (solid red line) and uplink (dashed black line) phase noise that correspond to labels (*b*) and (*d*) in Table I, respectively. The two-way phase noise difference [green (light gray line)] has zero mean with a variance of 0.69 rad^2.

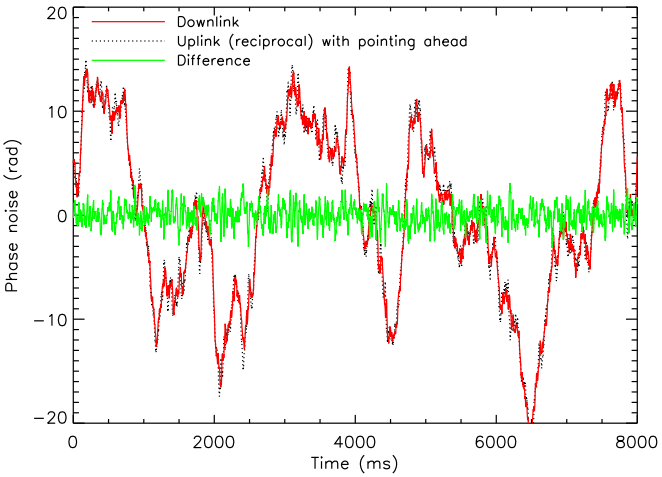

FIG. 14. Two-way compensation on phase noise in the case of asymmetrical apertures ($D_{1E} = 0.15$ m, $D_{1S} = 0.40$ m) with point ahead and with tip-tilt correction. Comparison between downlink (solid red line) and uplink (dashed black line) phase noise that corresponds to labels (*b*) and (*e*) in Table I, respectively. The two-way phase noise difference [green (light gray line)] has zero mean with a variance of 1.0 rad^2.

variances smaller than one square radian, that is much smaller than the variance on the individual links. Note that the structure of the residual phase noise is still different in the two cases: point ahead induces higher temporal frequencies. This can be explained by the fact that differential phase noise induced by point ahead mainly comes from the beam separation (paa times distance to ground) and therefore mainly originates from distant layers, associated with fast apparent winds, hence fast temporal evolution. Having the two asymmetries together (different apertures and point ahead), one obtains Fig. 14. Effects add up: The variance increases, and it is roughly the sum of the values found in the previous two cases. The residual phase noise has again high frequencies, as in Fig. 12, a direct consequence of point ahead.

It is now essential to present the main result for the frequency transfer community by looking at the corresponding modified Allan deviations (i.e., frequency stability). Figure 15 shows the modified Allan variance as a function of the averaging time for the various link asymmetries. The residual frequency stability with two-way compensation is in all cases around two orders of magnitude smaller than the one-way

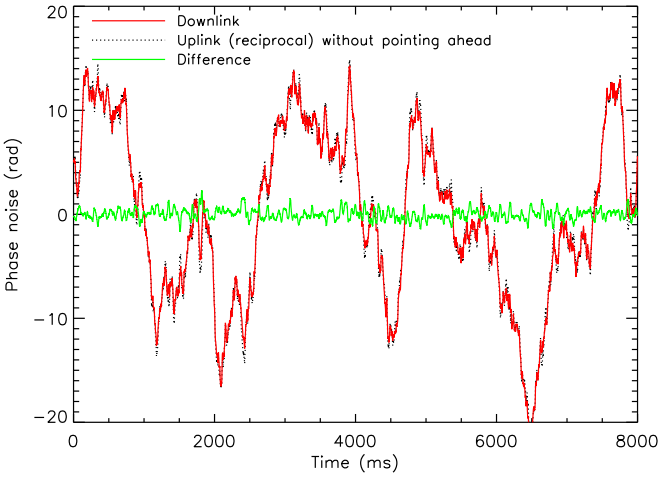

FIG. 13. Two-way compensation on phase noise in the case of asymmetrical apertures ($D_{1E} = 0.15$ m, $D_{1S} = 0.40$ m) without point ahead and with tip-tilt correction. Comparison between downlink (solid red line) and uplink (dashed black line) phase noise. Downlink corresponds to label (*b*) in Table I. Uplink mean heterodyne efficiency $\langle m \rangle = 0.79$ and its relative fluctuation $\sigma_m^2/\langle m \rangle^2 = 0.03$. The two-way phase noise difference [green (light gray line)] has zero mean with a variance of 0.27 rad^2.

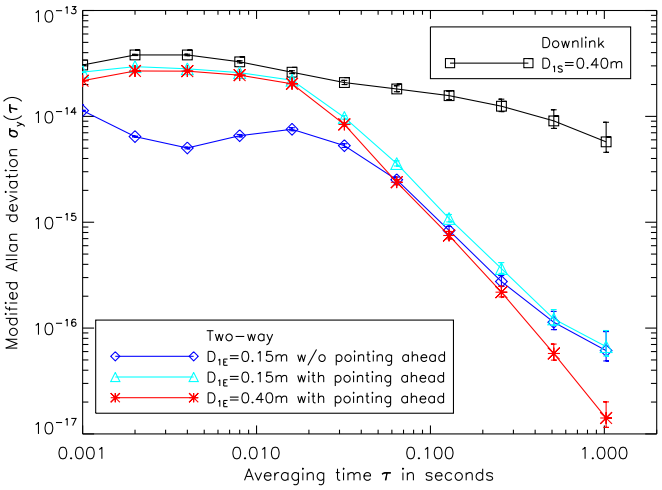

FIG. 15. Modified Allan variance as a function of the averaging time, for one-way downlink (squares) and two-way compensated link (diamonds, triangles, asterisks) vis-a-vis the various link asymmetries. All results are obtained with tip-tilt control and $D_{1S} = 0.40$ m. Two sigma error bars are displayed.

noise for long averaging times τ. More importantly, with two-way compensation, frequency stability averages as τ^{-1} or faster, while the one-way noise averages at best as $\tau^{-1/2}$. Furthermore, it becomes clear that the asymmetry from point ahead adds short term ($\tau \leqslant 0.3$ s) noise, while the asymmetry due to the difference in apertures adds long term noise ($\tau \geqslant 0.2$ s). Most time and frequency applications require long term ($\tau \geqslant 1$ s) stability; it is thus important to ensure the symmetry of the emission and LO modes on ground to get the best performance.

As an aside, we briefly consider link budget aspects. We recall that we assumed the largest diameter ($D_{1S} = 0.40$ m) for the ground terminal receiver, a choice often dictated by link budget constraints. The fact that best performance is obtained with an identical, hence large, emitter aperture leads to a small uplink beam divergence, that also helps the link budget. In such a system configuration, the reciprocity breakdown is only due to the point ahead, the effect of which remains minor. The Allan variance should be limited by other effects, such as signal-to-noise ratio, for instance.

Finally, we stress that the residual fractional frequency stability is as low as 1.410^{-17} after only 1-s averaging. Best clocks today have a stability of $\approx 10^{-16}/\tau^{-1/2}$ [42]. Therefore the turbulence-induced noise when comparing them by optical coherent satellite links becomes negligible for averaging times as short as a few seconds.

V. INFLUENCE OF TURBULENT PARAMETERS

In this final section we investigate the dependence of our results on different turbulent parameters like the Fried diameter r_0 or the outer scale L_0. We first discuss the influence of the turbulent outer scale L_0 on heterodyne efficiency, and two-way phase noise compensation still in moderate turbulence ($r_0 = 13$ cm). With an outer scale ranging from 2 to 10 m, mean and relative fluctuations of m vary by only a few percent. The effect of the outer scale on the standard deviation of two-way differential phase noise, for symmetric apertures $D_{1,S} = D_{1,E} = 0.40$ m, is given in Fig. 16. A slow increase is observed but differential phase noise variance remains smaller than $1\,\text{rad}^2$. Similar results are obtained with asymmetric apertures $D_{1,S} = 0.40$ m and $D_{1,E} = 0.15$ m. The turbulent outer scale is therefore not a very sensitive parameter, and other hypotheses on its value should therefore not strongly modify our results in terms of frequency stability.

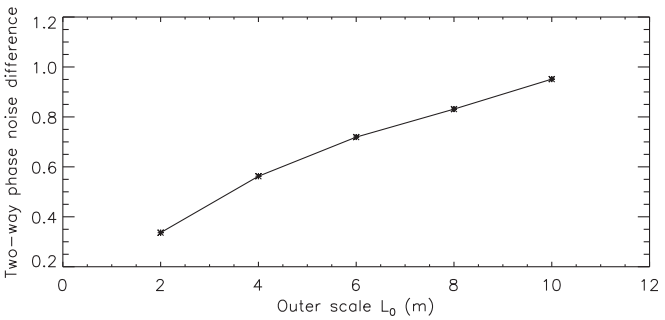

FIG. 16. Two-way phase noise difference (standard deviation in rad.) as a function of the outer scale value L_0 in meters.

We have considered so far moderate turbulence conditions with $r_0 = 13$ cm. We now study stronger turbulence conditions with a smaller Fried parameter of $r_0 = 5$ cm, still considering the same two aperture diameters $D = [0.15, 0.40]$ m, and always applying tip-tilt control. With a 0.40-m aperture, downlink and uplink give the same performance $\langle m \rangle = 0.09$ and $\sigma_m^2/\langle m \rangle^2 = 0.75$. Despite tip-tilt control, performance remains very poor, and we can show that extinctions become prohibitive in this case. To cope with these turbulence conditions, higher order adaptive optics can be considered, or more simply a reduction of the apertures if permitted by link budget considerations. With a 0.15-m aperture, we obtain $\langle m \rangle = 0.55$ and $\sigma_m^2/\langle m \rangle^2 = 0.07$ for the downlink, and $\langle m \rangle = 0.54$ and $\sigma_m^2/\langle m \rangle^2 = 0.07$ for the uplink. We remember that the key parameter is D/r_0; it is therefore not surprising that performance with moderate turbulence ($r_0 = 13$ cm) and 0.40-m aperture [cases with labels (b) and (d) in Table I] is similar to that with strong turbulence ($r_0 = 5$ cm) and 0.15-m aperture since in both cases $D/r_0 \approx 3$. We have checked also the similarity in terms of phase noise. The structure of phase noise, and differential phase noise, with strong turbulence ($r_0 = 5$ cm) and 0.15-m apertures indeed resembles that of Fig. 12, with a comparable standard deviation of the differential phase noise, 0.86 rad in place of 0.83 rad.

Note that two-way compensation does not only depend on the global turbulence strength, characterized by the Fried parameter, but also on the vertical distribution of turbulence, the C_n^2 profile. Of course, having stronger turbulence in the upper layers would lead to a larger angular decorrelation of turbulence, and in turn would increase the point-ahead impact. Turbulence effects are evaluated here for a standard Hufnagel-Valley profile in the case of a ground station on an astronomical site. Even though out of the scope of the present article, the formalism developed here allows one to perform a quantitative analysis for any profile coming from either models or from experimental measurements (see, for instance, [43] and references therein).

VI. CONCLUSION

This article studies the effect of atmospheric turbulence on frequency transfer through bidirectional ground-satellite laser links. After recalling the effect of turbulence on heterodyne efficiency (reduction of mean value and fluctuations leading possibly to extinctions), we give a comprehensive theoretical analysis of the notion of link reciprocity in our context, with a particular emphasis on phase noise. The principle of reciprocity allows a reformulation of the down- and uplink performance based on the propagation of two downward plane waves separated by the point-ahead angle. This powerful formulation enables a very clear understanding of the physical nature of the phase noise on both channels. It becomes, for instance, obvious that two-way phase noise compensation is ultimately limited by the asymmetries of the link: point-ahead effect and possibly differences between reception and emission aperture of the ground terminal.

At this point the question was whether turbulent effects together with link asymmetries (point ahead, aperture asymmetry) were a strong limiting factor for high-precision frequency transfer in two-way configurations. We address this

point through a refined end-to-end simulation under realistic turbulence and satellite kinematics, accounting for point ahead.

We show that tip-tilt control is mandatory on the ground terminal to maintain reasonable signal-to-noise ratio and avoid frequent and severe extinctions, even at astronomical sites under intermediate turbulence. Tip-tilt control is applied to correct the downlink and pre-compensate the uplink. Despite a point-ahead angle larger than the isoplanatic angle, tip-tilt correction is shown to be efficient on the uplink. Operating with stronger turbulence would require one to reduce the ground terminal apertures (typically so that $D \leqslant 3r_0$), if permitted by other system considerations, or to implement higher order adaptive optics correction, keeping in mind that point ahead may limit pre-compensation capabilities for the uplink.

Phase noise is shown to remain highly reciprocal, that is, with a good correlation between up and down phase noise, despite point-ahead and ground aperture asymmetry. Two-way phase noise compensation is therefore very efficient and leads to a two-way differential phase noise with a residual variance at the $1\,\mathrm{rad}^2$ level. This translates to very good performance in terms of fractional frequency stability that is quantified by the modified Allan variance. Asymmetry from point ahead is shown to dominate at short term, asymmetry from apertures at long term. The best performance is obtained with identical apertures, meaning identical local oscillator and emission modes on the ground terminal. Essentially, we quantify the residual phase noise between the up- and downlink, showing that a frequency stability better than 2×10^{-17} with only a 1-s averaging time is possible, with good prospects of reaching sub-10^{-18} levels after a few minutes averaging. This outstanding performance is very promising for high-precision ground-satellite frequency transfer with two-way coherent optical links, and turbulence is certainly not a strong limiting factor.

ACKNOWLEDGMENTS

This work has been funded by the French Space Agency Centre National d'Etudes Spatiales (CNES) following the preliminary HPFDIS study performed for European Space Agency (ESA). The authors thank also Marie-Thérèse Velluet, Nicolas Védrenne, and Vincent Michau for the fruitful exchanges they have had with them. We appreciate the anonymous reviewer for his numerous valuable comments that helped to improve the manuscript.

[1] S. Seel, H. Kämpfner, F. Heine, D. Dallmann, G. Muhlnikel, M. Gregory, M. Reinhardt, K. Saucke, J. Muckherjee, U. Sterr, B. Wandernoth, R. Meyer, and R. Czichy, Space to ground bidirectional optical communication link at 5.6 Gbps and EDRS connectivity outlook, in *Aerospace Conference, 2011 IEEE* (IEEE, Piscataway, 2011), pp. 1–7.

[2] B. Christophe, L. J. Spilker, J. D. Anderson, N. André, S. W. Asmar *et al.*, OSS (Outer Solar System): A fundamental and planetary physics mission to Neptune, Triton and the Kuiper Belt, Exper. Astron. **34**, 203 (2012).

[3] P. Wolf, Quantum physics exploring gravity in the outer solar system: the SAGAS project, Exper. Astron. **23**, 651 (2009).

[4] http://sci.esa.int/ste-quest/

[5] S. Reynaud, B. Lamine, L. Duchayne, P. Wolf, and M.-T. Jaekel, Bounds on Gravitational Wave Backgrounds from Large Distance Clock Comparisons, Phys. Rev. D **77**, 122003 (2008).

[6] O. Lopez, A. Haboucha, B. Chanteau, C. Chardonnet, A. Amy-Klein, and G. Santarelli, Ultra-stable long distance optical frequency distribution using the Internet fiber network, Opt. Express **20**, 23518 (2012).

[7] K. Predehl, G. Grosche, S. M. F. Raupach, S. Droste, O. Terra, T. Alnis, J. Legero, T. W. Hänsch, T. Udem, and R. Holzwarth, A 920-kilometer optical fiber link for frequency metrology at the 19th decimal place, Science **336**, 441 (2012).

[8] K. Djerroud, O. Acef, A. Clairon, P. Lemonde, C. N. Man, E. Samain, and P. Wolf, Coherent optical link through the turbulent atmosphere, Opt. Lett. **35**, 1479 (2010).

[9] F. R. Giorgetta, W. C. Swann, L. C. Sinclair, E. Baumann, I. Coddington, and N. R. Newbury, Optical two-way time and frequency transfer over free space, Nat. Photon. **7**, 434 (2013).

[10] L. C. Sinclair, F. R. Giorgetta, W. C. Swann, E. Baumann, I. Coddington, and N. R. Newbury, Optical phase noise from atmospheric fluctuations and its impact on optical time-frequency transfer, Phys. Rev. A **89**, 023805 (2014).

[11] D. L. Fried, Optical heterodyne detection of an atmospherically distorted signal wave front, Proc. IEEE **55**, 57 (1967).

[12] J. H. Churnside, and C. M. McIntyre, Signal current probability distribution for optical heterodyne receivers in the turbulent atmosphere. 1: Theory, Appl. Opt. **17**, 2141 (1978).

[13] K. A. Winick, Atmospheric turbulence-induced signal fades on optical heterodyne communication links, Appl. Opt. **25**, 1817 (1986).

[14] J. E. Kaufmann, in *Performance Limits of High-Rate Space-to-Ground Optical Communications through the Turbulent Atmospheric Channel* (SPIE, Bellingham, 1995), Vol. 2381, pp. 171–182.

[15] N. Perlot, Turbulence-induced fading probability in coherent optical communication through the atmosphere, Appl. Opt. **46**, 7218 (2007).

[16] A. Belmonte, Influence of atmospheric phase compensation on optical heterodyne power measurements, Opt. Express **16**, 6756 (2008).

[17] A. Belmonte and J. Khan, Performance of synchronous optical receivers using atmospheric compensation techniques, Opt. Express **16**, 14151 (2008).

[18] J. H. Shapiro, Reciprocity of the turbulent atmosphere, JOSA **61**, 492 (1971).

[19] R. Lutomirski and H. Yura, Propagation of a finite optical beam in an inhomogeneous medium, Appl. Opt. **10**, 1652 (1971).

[20] H. T. Yura and D. L. Fried, *Telescope Performance Reciprocity for Propagation in a Turbulent Medium, DTIC Document* (Defense Technical Information Center, Fort Belvoir, 1972).

[21] J. H. Shapiro, Normal-mode approach to wave propagation in the turbulent atmosphere, Appl. Opt. **13**, 2614 (1974).
[22] J. H. Shapiro, Point-ahead limitation on reciprocity tracking, JOSA **65**, 65 (1975).
[23] J. Shapiro, Imaging and optical communication through atmospheric turbulence, in *Laser Beam Propagation in the Atmosphere* (Springer, New York, 1978), pp. 171–222.
[24] J. H. Shapiro, and A. L. Puryear, Reciprocity-enhanced optical communication through atmospheric turbulence. Part I: Reciprocity proofs and far-field power transfer optimization, Opt. Commun. Netw. **4**, 947 (2012).
[25] A. L. Puryear, J. H. Shapiro, and R. R. Parenti, Reciprocity-enhanced optical communication through atmospheric turbulence. Part II: Communication architectures and performance, Opt. Commun. Netw. **5**, 888 (2013).
[26] R. R. Parenti, J. M. Roth, J. H. Shapiro, F. G. Walther, and J. A. Greco, Experimental observations of channel reciprocity in single-mode free-space optical links, Opt. Express **20**, 21635 (2012).
[27] D. Giggenbach, W. Cowley, K. Grant, and N. Perlot, Experimental verification of the limits of optical channel intensity reciprocity, Appl. Opt. **51**, 3145 (2012).
[28] J. Minet, M. A. Vorontsov, E. Polnau, and D. Dolfi, Enhanced correlation of received power-signal fluctuations in bidirectional optical links, J. Opt. **15**, 022401 (2013).
[29] Edited by F. Roddier, *Adaptive Optics in Astronomy* (Cambridge University Press, Cambridge, 1999).
[30] C. Ruilier and F. Cassaing, Coupling of large telescopes and single-mode waveguides: Application to stellar interferometry, J. Opt. Soc. Am. A **18**, 143 (2001).
[31] S. Meimon, F. Cassaing, and G. Prévôt, Experimental study of distorted beams coupling in a single mode waveguide, J. Opt. **15**, 035707 (2013).
[32] http://tf.nist.gov/time/twoway.htm
[33] H. Hemmati, *Near-Earth Laser Communications* (CRC Press, Boca Raton, 2009).
[34] C. Robert, J.-M. Conan, V. Michau, T. Fusco, and N. Védrenne, Scintillation and phase anisoplanatism in Shack-Hartmann wavefront sensing, J. Opt. Soc. Am. A **23**, 613 (2006).
[35] N. Védrenne, J.-M. Conan, M.-T. Velluet, M. Séchaud, M. Toyoshima, H. Takenaka, A. Guérin, and F. Lacoste, Turbulence effects on bi-directional ground-to-satellite laser communication systems, in *ICSOS Proceedings for International Conference on Space Optical Systems and Applications (ICSOS) (2012)* (Corsica, France, 2012).
[36] M.-T. Velluet, S. Gousset, and N. Védrenne, Optical links between ground to space: propagation channel study, in *Applications of Lasers for Sensing and Free Space Communications* (Optical Society of America, Washington, DC, 2015), pp. LTh2D–1.
[37] http://commons.wikimedia.org/wiki/File:UFO_satellite_2.jpg
[38] A. Ziad, M. Schöck, G. A. Chanan, M. Troy, R. Dekany, B. F. Lane, J. Borgnino, and F. Martin, Comparison of measurements of the outer scale of turbulence by three different techniques, Appl. Opt. **43**, 2316 (2004).
[39] C. Coulman, J. Vernin, Y. Coqueugniot, and J. Caccia, Outer scale of turbulence appropriate to modeling refractive-index structure profiles, Appl. Opt. **27**, 155 (1988).
[40] F. Chassat, Theoretical evaluation of the isoplanatic patch of an adaptive optics system working through the atmospheric turbulence, J. Opt. **20**, 13 (1989).
[41] J.-M. Conan, G. Rousset, and P.-Y. Madec, Wave-front temporal spectra in high-resolution imaging through turbulence, J. Opt. Soc. Am. A **12**, 1559 (1995).
[42] T. Nicholson, S. Campbell, R. Hutson, G. Marti, B. Bloom, R. McNally, W. Zhang, M. Barrett, M. Safronova, G. Strouse *et al.*, Systematic evaluation of an atomic clock at 2×10^{-18} total uncertainty, Nat. Commun. **6**, 6896 (2015).
[43] J. Voyez, C. Robert, J.-M. Conan, L. M. Mugnier, E. Samain, and A. Ziad, First on-sky results of the CO-SLIDAR C_n^2 profiler, Opt. Express **22**, 10948 (2014).